ADVANCED FUNCTIONAL MATERIALS
www.afm-journal.de

Tunable Self-Assembled Micro/Nanostructures of Carboxyl-Functionalized Squarylium Cyanine for Ammonia Sensing

*Jie Li, Baozhong Lv, Dongpeng Yan, Shouke Yan, Min Wei, and Meizhen Yin**

Orderly molecular self-assembly for tunable micro/nanostructures is an effective way to prepare novel functional materials with desired properties. Squarylium cyanine (SCy) dyes have received great attention in the fields of laser, imaging, and optoelectronic device. However, the detailed self-assembly behavior of SCy has rarely been investigated. In the present work, two SCy derivatives, D1 and D2, respectively, bearing four and two carboxylic acid groups at different positions are prepared and used as a model system to investigate the molecular self-assembly, morphology, and optical properties of SCy dyes. The hydrogen-bonding interactions between the carboxylic acid groups in D1 and D2 are determined with X-ray diffraction, 2D nuclear magnetic resonance, and Fourier transformation infrared spectroscopy. The two types of hydrogen bonds in D1 cooperating with inherent π–π stacking interaction result in tunable molecular aggregations, which further leads to the transformation between *J*-aggregation and *H*-aggregation of D1 in the solid state in response to ammonia gas. In all, this work provides a feasible and effective way to study the self-assembled aggregates of SCy dyes at both molecular and supramolecular levels, and has developed a reversible sensor for ammonia gas detection.

1. Introduction

In the past five decades, molecular self-assembly has received considerable attentions because it can promote the transformation from disorder to order in nature and provide an efficient and convenient "bottom up" means for the fabrication of molecular micro/nanostructures.[1] Among all self-assembly units, carboxylic acid group has been particularly studied due to its high reactivity and intriguing noncovalent inter/intramolecular hydrogen-bonding capability and coordination with metals.[2] For example, organic dyes containing carboxylic acid groups have been prepared as building blocks to construct organometallic complex and metal organic framework (MOF) for sensors or as catalysts.[3] The coordination between the carboxylic acid groups with metal ions[4] and the inter/intramolecular hydrogen-bonding interactions of carboxylic acid groups[5] can be determined simply by monitoring the change in their optical spectra.

Squarylium dyes have been widely used due to their high absorbance and emission efficiency in visible and/or near infrared regions.[6] Squarylium cyanine (SCy) dyes containing carboxylic acid group have also been thoroughly investigated for diverse applications. For example, Nazeeruddin and co-workers introduced carboxylic acid groups into the indoline moiety of SCy dye and used the modified SCy dye as an anchor for TiO_2 toward dye-sensitized solar cells.[7] It is believed that the carboxylic acid group can significantly affect the aggregation behaviors of SCy dyes. However, to the best of our knowledge, the detailed aggregation behaviors of SCy dyes caused by carboxylic acid groups as well as their related optical/luminescent properties have not been reported. Additionally, the aggregated types of *H*-aggregation or *J*-aggregation could highly affect the performance of the functional materials. Interestingly, some research groups have found that the *H*-aggregation and *J*-aggregation can be transformed by adding small molecules or changing the environment.[8] This transformation can significantly change the optical spectra of aggregates and cause fluorescence emission or quenching.

In the present work, SCy derivatives were prepared by introducing different numbers of carboxylic acid groups to the conjugated indoline moiety and/or the terminal group of alkylating agent (**Scheme 1**, **D1** and **D2**). The influence of carboxylic acid group on the self-assembling behavior of the SCy dyes was investigated with scanning electron microscopy (SEM), 2D nuclear magnetic resonance (NMR), X-ray diffraction (XRD), and Fourier transformation infrared (FTIR) spectroscopy. The results indicate that carboxylic acid groups affect the self-assembling behavior of SCy dyes due to the formation of different hydrogen bonds. The morphologies of the SCy micro/nanoparticles can be tuned by adjusting its solution concentrations. The unique architectures of **D1** and **D2** can be attributed to the hydrogen-bonding interactions

J. Li, B. Lv, Prof. D. Yan, Prof. S. Yan, Prof. M. Wei, Prof. M. Yin
State Key Laboratory of Chemical Resource Engineering
Key Laboratory of Carbon Fiber and Functional Polymers of Ministry of Education
Beijing Laboratory of Biomedical Materials
Beijing University of Chemical Technology
Beijing 100029, P. R. China
E-mail: yinmz@mail.buct.edu.cn

DOI: 10.1002/adfm.201503825

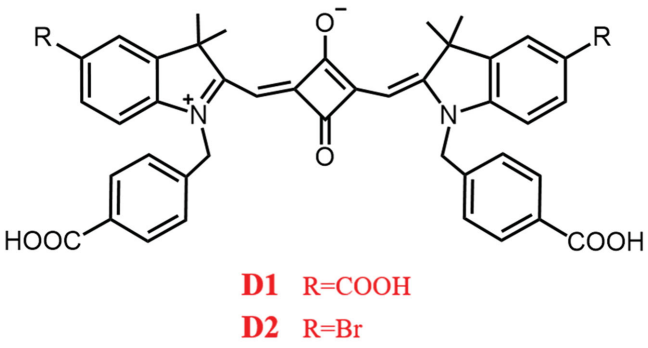

Scheme 1. The structures of squarylium cyanine bearing four (**D1**) and two (**D2**) carboxylic acid groups.

between the carboxylic acid groups and π–π stacking of the conjugated SCy dyes (**Scheme 2** and Scheme S1, Supporting Information). Interestingly, the **D1** aggregates in the solid state showed a reversible selective response to ammonia gas by monitoring the change in its UV–vis absorption spectrum. It can be explained that the ammonia broke the carboxylic acid dimers, leading to the relative sliding between **D1** molecules. The aggregation state of **D1** was then reversibly transformed between *H*-aggregation and *J*-aggregation upon the absorption/desorption of ammonia gas. Our work provides a platform for the investigation of the influence of carboxylic acid group on the self-assembling behavior of SCy dyes as well as a promising optical sensor for ammonia gas detection.

2. Results and Discussion

SCy dyes bearing four and two carboxylic acid groups (**D1** and **D2**) were prepared. **D1** containing four carboxylic acid groups on the horizontal direction showed strong hydrogen-bonding tendency. While, **D2** bearing two carboxylic acid groups and two bromine groups exhibited lower hydrogen-bonding ability than **D1**. Their concentration-dependent UV–vis absorption and fluorescence emission spectra in *N*,*N*′-dimethylformamide (DMF) solution were determined (**Figure 1A** and Figure S1A, Supporting Information). The maximum absorbance and fluorescence emission of **D1** or **D2** solution (1×10^{-6} M) were found at 637 and 647 nm, respectively. As the concentration increased from 1×10^{-6} to 10×10^{-6} M, a new redshifted emission peak appeared at ≈715 nm. The redshift of the emission peaks can be attributed to the *J*-aggregations of **D1** and **D2** at high concentration.[9] Figure 1B and Figure S1B (Supporting Information) show the corresponding UV–vis absorption and fluorescence emission spectra of **D1** and **D2**, respectively, after the solvent was evaporated. Compared with their absorbance in solution, the absorbances of both **D1** and **D2** in the solid state were significantly redshifted. In addition, their fluorescence emissions at 715 nm were dramatically increased, which was attributed to their new aggregation state. These results indicate that the SCy dyes tend to form *J*-aggregation at high concentration and the carboxylic acid groups on SCy dyes have no significant effect on their optical properties.

To investigate the influence of carboxylic acid group on the self-assembling behavior of SCy dyes, the morphologies of SCy dyes in the solid state were imaged with SEM and

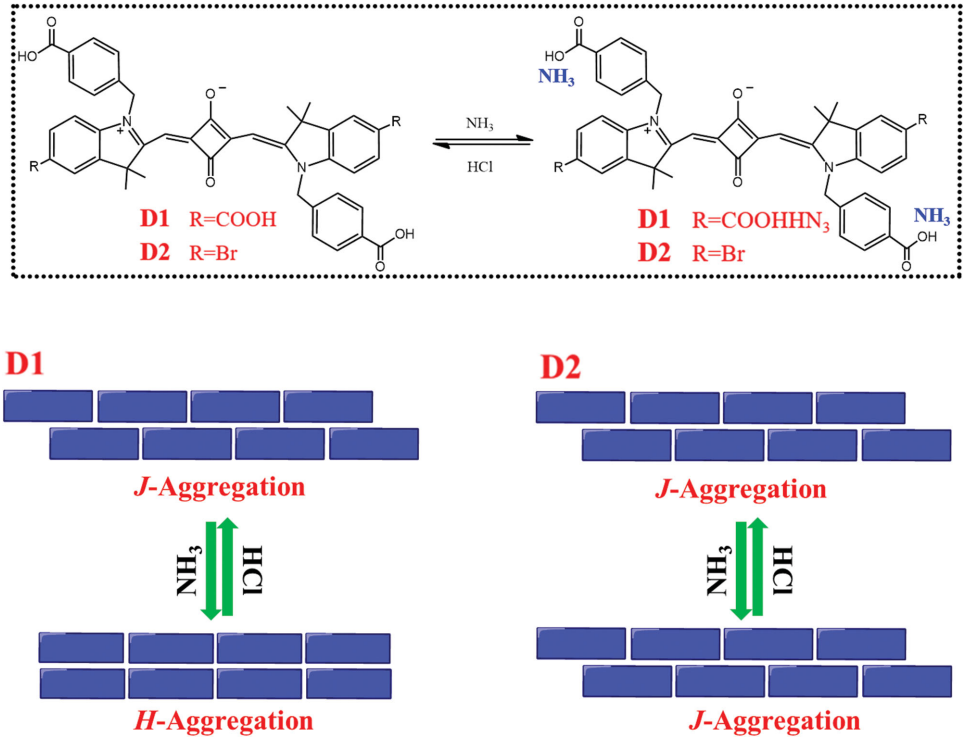

Scheme 2. The mechanism of concentration-dependent self-assembly of SCy dyes in the solid state for selective ammonia gas sensing.

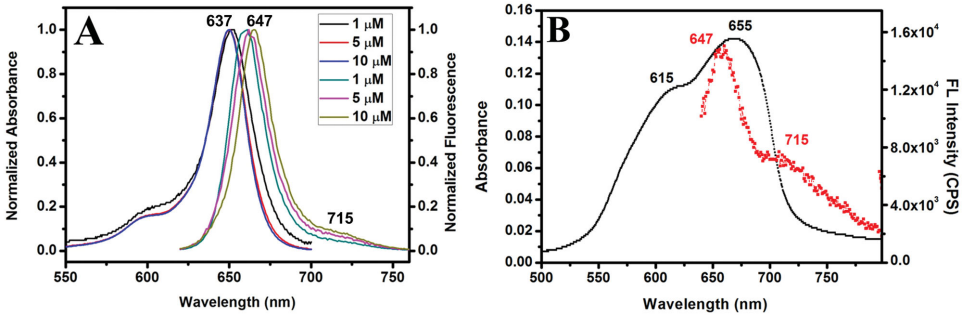

Figure 1. A) Concentration-dependent UV–vis absorption and fluorescence emission spectra of **D1** in DMF solution at the concentrations of 1×10^{-6}, 5×10^{-6}, and 10×10^{-6} M. B) UV–vis absorption and fluorescence emission spectra of **D1** after DMF was evaporated.

high-resolution transmission electron microscopy (HRTEM) after the solvent was evaporated. The dyes showed a concentration-dependent aggregation characteristic. A uniform rod-like structure of **D1** with a width of 110 nm was formed in its 10×10^{-6} M DMF solution and microsheets with the widths of 2.5–3 μm were obtained as the concentration increased to 1×10^{-3} M (**Figure 2**A,B). The microparticles of **D2** formed at 10×10^{-6} M were nanospheres with sizes of 50–70 nm, which were changed into ellipsoids with the length of ≈1 μm as the concentration increased to 1×10^{-3} M (Figure 2C,D). These results indicate that the number and position of carboxylic acid groups play an important role in the self-assembly of SCy dyes.

The fine structures of **D1** and **D2** aggregated nanoparticles in the solid state were also revealed by HRTEM (**Figure 3**). Nanorods were observed in **D1** solution with the concentration of 10×10^{-6} M (Figure 3A), and nanospheres were found in **D2** solution with the concentration of 100×10^{-6} M (Figure 3B). Both nanostructures displayed high-resolution lattice fringes (inset in Figure 3), indicating the occurrence of highly oriented self-assembly in the long-axis direction. The crystalline interplanar spacings for the nanorod and nanosphere were estimated as 0.39 and 0.18 nm, respectively. To confirm the oriented micro/nanostructures of **D1** and **D2**, their anisotropies were determined with polarizing optical microscopy (POM) (**Figure 4**). The fluorescence intensities of both microsheets (Figure 4a1,a2) and micro-ellipsoids (Figure 4b1,b2) were changed significantly after a deflection of 45°, indicating the highly oriented crystalline structures of both **D1** and **D2** micro/nanoaggregates.

We hypothesized that the carboxylic acid group and π–π stacking synergistically contributed to the diverse morphologies of the aggregates of SCy dyes. The aggregation of SCy dyes can then be further investigated by 2D NMR since the protons separated from each other have a spatial distance less than 0.5 nm and lead to a cross-peak in their rotating-frame Overhauser effect spectroscopy (ROESY) NMR spectra.[10] Well separated and sharp peaks of SCy dyes were observed in the ^{1}H NMR spectra of both **D1** and **D2** (Figures S2 and S3, Supporting Information), which is an ideal model for investigating the aggregation process. The cross-peaks of H9 with H2, H7 with H6 and H9, and H8 with H5 and H6 were observed in the ROESY NMR spctrum of **D1** (**Figure 5**A). As discussed above, the protons in the SCy dyes are well separated from each other. The cross-peaks can be attributed to the intermolecular interactions between the neighboring SCy molecule and the π–π stacking is the driving force to form the aggregation in close proximity.[11] Similar conclusion was obtained from the 2D NMR analysis of **D2** (Figure 5B). It is noted that the proton in carboxylic acid group is highly active, and thus no cross-peak of intermolecular hydrogen bonds was observed.

Figure 6 and Figure S4 (Supporting Information) are the FTIR spectra of **D1** and **D2** in the selected and whole ranges, respectively. It has been reported that the maximum absorption of free C=O stretching of both carboxylic acids and squaric acids is at ≈1735 cm^{-1}.[12] No peak was observed at ≈1735 cm^{-1} in either of the spectra of **D1** or **D2**, indicating the occurrence of the interaction between the carbonyl groups. The characteristic vibration bands

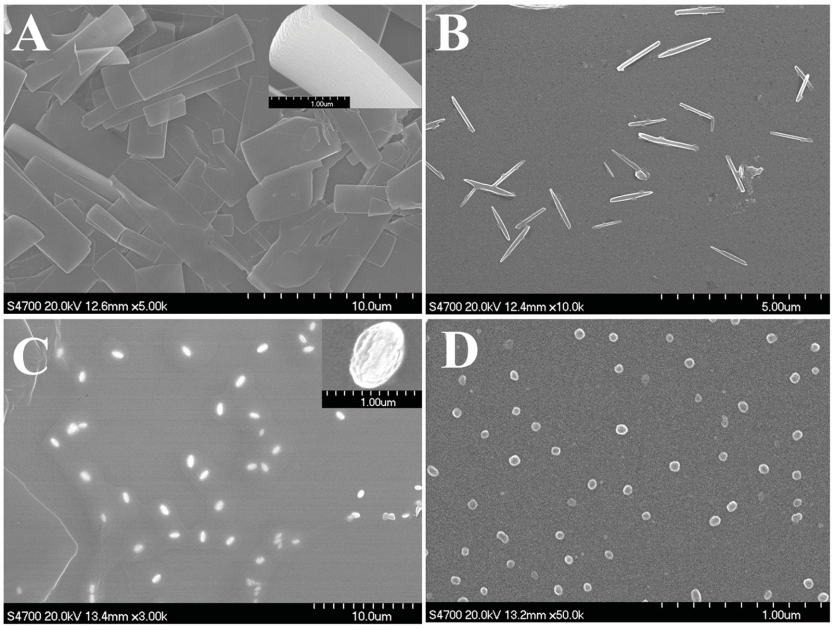

Figure 2. Concentration-dependent morphologies of A,B) **D1** and C,D) **D2**. The SEM imaging was conducted by evaporating the A,C) 1×10^{-3} M and B,D) 10×10^{-6} M DMF solutions on a glass slide. The insets in (A) and (C) are the amplified images of selected particles.

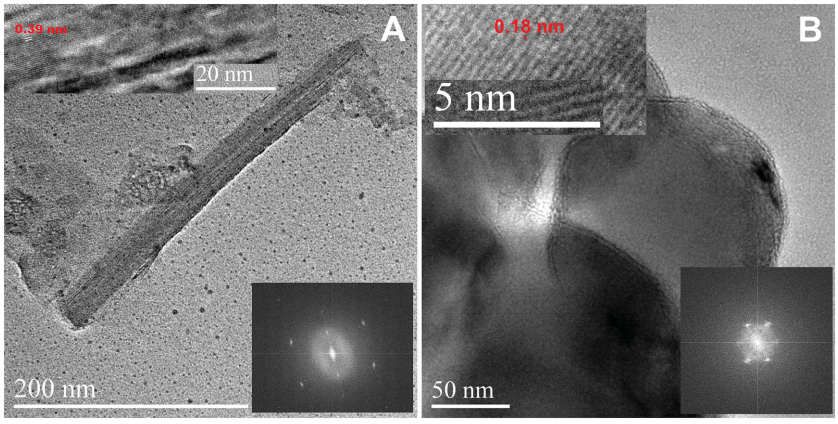

Figure 3. HRTEM micrographs of A) **D1** and B) **D2** aggregates. The top left insets are the partially enlarged views of the frame selected area. The bottom right insets are the diffraction patterns of selected area. The concentrations of **D1** and **D2** solutions were 10×10^{-6} and 100×10^{-6} M, respectively.

for the hydrogen bond between the two carboxylic acids of the dimer, OH stretching and carbonyl stretching were observed at 2628, 2504, and 1679 cm^{-1}, respectively, in the spectrum of **D1**.[13] Another charateristic vibration band at ≈1703 cm^{-1} can be assigned to the stretching vibration of the hydrogen-bonded carbonyl group between the carboxylic acid groups and the carbonyl group of squaric acid.[14] The charateristic vibration band of the carbonyl group of **D2** was observed at 1703 cm^{-1}, indicating that the hydrogen bonding between the carboxylic acid and squaric acid contributed to the aggregation of **D2**.

To confirm the hydrogen bonding in/between SCy dyes, sodium carboxylate of **D1** was prepared (denoted as **D3**) and characterized with FTIR. The characteristic vibration band of carboxylate group of **D3** appeared at 1555 cm^{-1} and the characteristic vibration bands of the carbonyl group involved in hydrogen bonding at 1703 and 1679 cm^{-1} disappeard (Figure S5, Supporting Information). The characteristic vibration bands of carbonyl group of squaric acid shifted to 1713 cm^{-1} due to the released carbonyl groups from the hydrogen bonds. The results from FTIR and ROESY NMR spectra demonstrate that both hydrogen bonding and π–π stacking contribute to the self-assembly of SCy dyes. The hydrogen bondings in **D1** and **D2** lead to the the distinct *J*-aggregation.

Next, powder XRD was conducted on both **D1** and **D2** to explore their self-assembly mechanism. With the aid of structural solving and refinement,[15] all reflection peaks of the as-obtained **D1** and **D2** were simulated and indexed to a triclinic lattice (**Figure 7**A,B). The simulated reflection peaks of both **D1** and **D2** are well consistent with the experimental results, indicating that the simulated structures fit well with the experimental structures of **D1** and **D2** aggregates. The typical molecular geometries of **D1** and **D2** consisting of four molecular units are shown in Figure 7C,D, respectively.

Two hydrogen-bonding interactions were found in **D1**, including the hydrogen bonding between the carboxylic acids in the dimer with a distance of 0.2 nm and that between carboxylic acid group and the carbonyl group of squaric acid with a distance of 0.425 nm. In contrast, only one type of hydrogen bonding was found in **D2**, which was formed between the carboxylic acid group and the carbonyl group of squaric acid

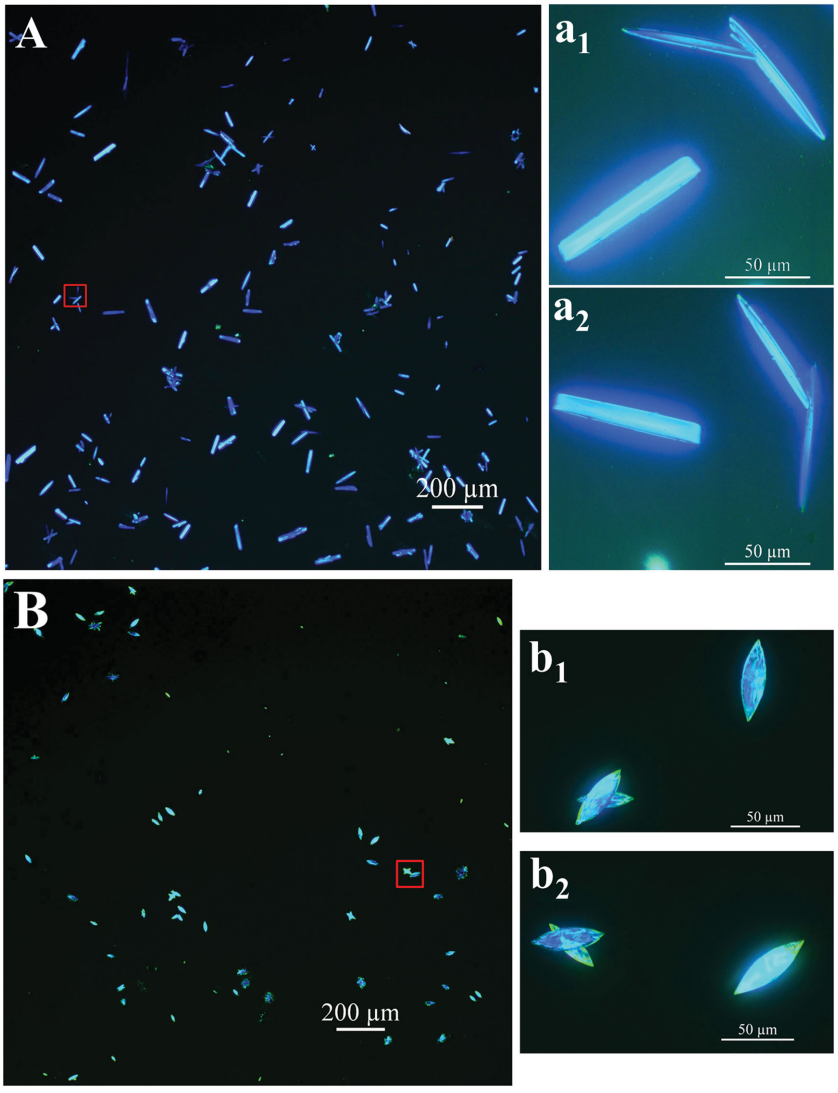

Figure 4. POM images of A,a_1,a_2) **D1** and B,b_1,b_2) **D2**. a_1,a_2) Partially enlarged views of the selected area in (A). b_1,b_2) Partially enlarged views of the selected area in (B). (a_2) and (b_2) are the corresponding visions of 45° deflection of (a_1) and (b_1), respectively.

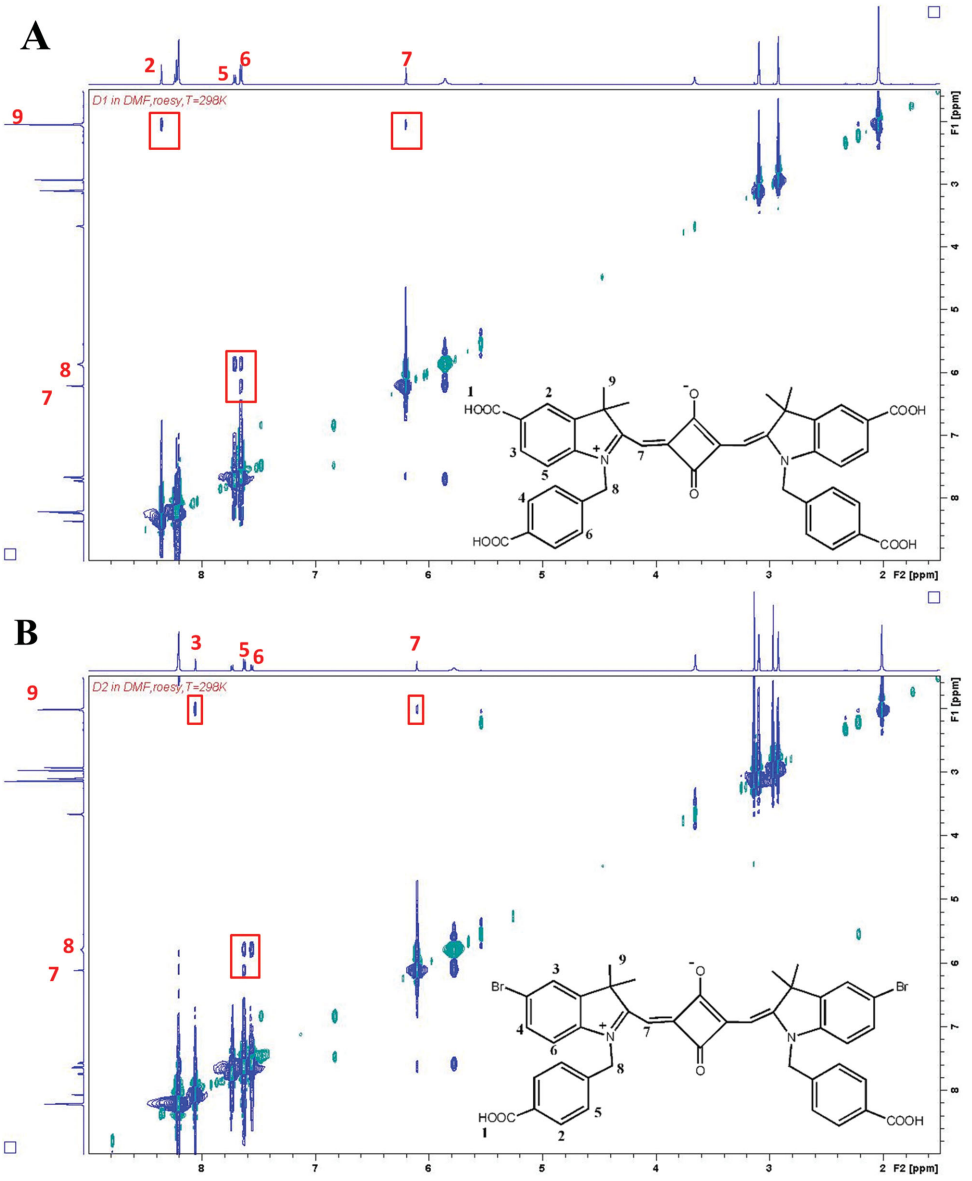

Figure 5. ROESY NMR spectra of A) **D1** (c = 10^{-3} M) and B) **D2** (c = 10^{-3} M) in [D_7] DMF.

with two distances of 0.298 and 0.344 nm. The modeling result demonstrates that both **D1** and **D2** feature *trans*-form π–π stacking in the *J*-aggregation, and different hydrogen bonds are formed during the self-assembly, consistent with the results of 2D NMR spectra and FTIR analyses as described above.

The detection of basic gases, especially with the widely used ammonia gas, on a small quantities are important for studying the air pollution owing to the harmful basic gases. The reported ammonia gas sensor are mostly based on the MOF or hybrid structures and their processes are relatively complex.[16] Generally, basic gas can be selectively absorbed on the self-assembled structures constructed by the hydrogen bonding of carboxylic acid groups via electrostatic interaction, resulting in alternated electronic structures.[17] Here, we checked the changes of the UV–vis absorption spectra of **D1** and **D2** in the solid state upon the treatments with different basic gases. As shown in **Figure 8**A, **D1** selectively responses to ammonia gas. The maximum absorbance of **D1** shifted from 670 to 610 nm with a new peak arising at 550 nm upon the treatment with ammonia gas and then shifted back to 670 nm with the disapearance of the peak at 550 nm after the ammonia adsorbed **D1** was treated with HCl gas. The concentration limitation of ammonia gas reaches to 60 ppm (Figure S6, Supporting Information). In constrast, no change was found in the UV–vis absorption spectrum of **D2** when it was treated with ammonia gas. In addition, neither of **D1** or **D2** showed any response to other basic gases including ethanediamine and aniline gas (Figure S7, Supporting Information). The mechanism of the selective response of **D1** to ammonia was then invesitgated.

As discussed above, the maximum absorption peaks of **D1** and ammonia adsorbed **D1** were found at 670 and 610 nm, which were attributed to *J*-aggregation and *H*-aggregation,

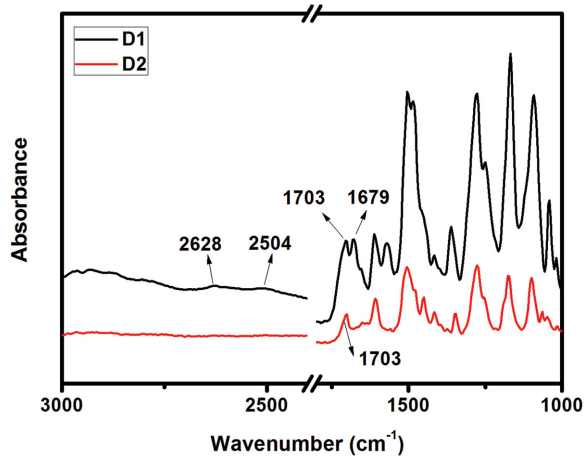

Figure 6. FTIR spectra of **D1** (red) and **D2** (black) in the regions of 3000–2400 and 1800–1000 cm^{-1} at room tempurature.

respectively.[18] The tranformation between the aggregation states and the selective response to ammonia gas of **D1** in the solid state may be highly dependent on the size of the basic gase, which has been proved as an important factor for the gas adsorption on a solid phase.[19] The molecular sizes of ammonia, thanediamine, and aniline were calculated as ≈0.15, ≈0.71, and ≈0.59 nm, respectively (**Figure 9**).

It is clear that the radius of ammonia molecule (0.15 nm) is smaller than the distance of the hydrogen bonds of **D1** (0.2 or 0.425 nm) and can easily enter the hydrogen-bonding network. The sizes of ethanediamine and aniline molecules are as big as ≈0.71 and 0.59 nm, respectively, which inhibit their entering into the hydrogen-bonding network of the aggregated **D1**. In addition, as shown in Figure 7C,D, **D1** network is much easier to slide than **D2** network when the hydrogen bonds are broken. As a result, **D1** was changed from *J*-aggregation to *H*-aggregation after treated with ammonia gas, while the interlaced aggregation state of **D2** remained unchanged upon the same treatment. The *H*-aggregation of **D1** was switched back to *J*-aggregation when the hydrogen bonding was reformed by neutralizing the ammonia with HCl. These results indicate that the molecular self-assembled structures and the size of the basic gas endow the specific response of **D1** to ammonia gas.

3. Conclusion

In summary, SCy dyes (**D1** and **D2**) containing different numbers of carboxylic acid groups were prepared and used to fabricate self-assembled micro/nanostructures. The carboxylic acid group can significantly affect the molecular self-assembling behaviors of SCy dyes. Two types of hydrogen bonding, including the hydrogen binding between the two carboxylic acids in the dimer and that between carboxylic acid and the carbonyl group of squaric acid, were formed in/between **D1** that bears four carboxylic acid groups. Therefore, **D1** tends to form the aggregates of 2D microsheets and 1D nanorods at high and low concenrtrations, respectively. **D2** that bears two carboxylic acid groups features one type of hydrogen bonding between the

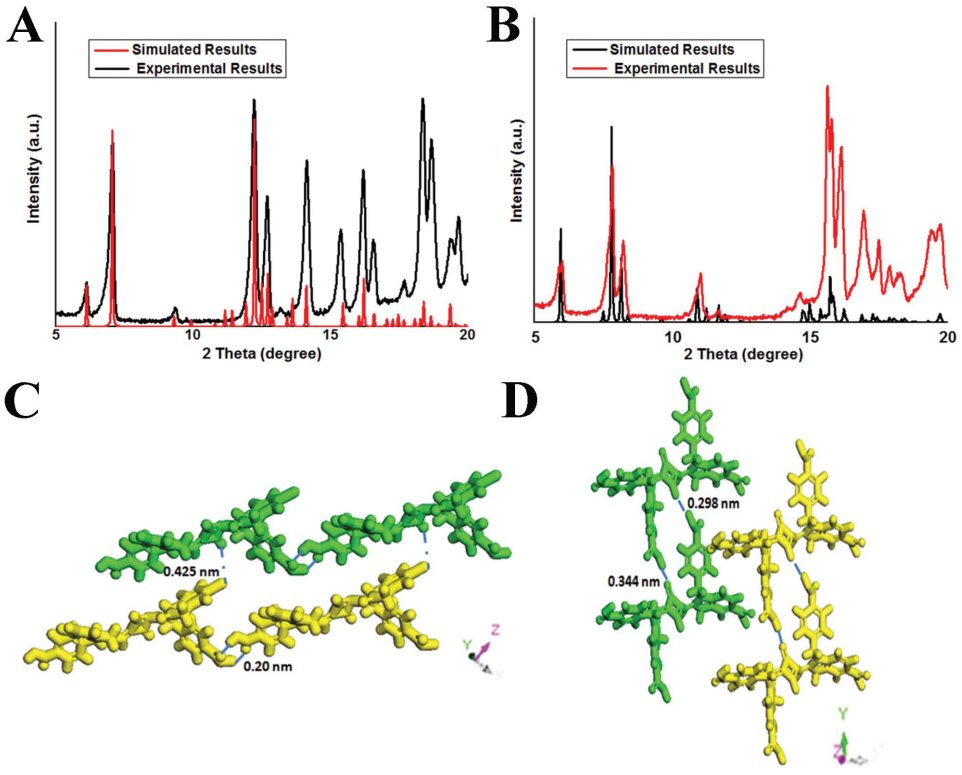

Figure 7. A) Experimental and simulated powder XRD profiles of **D1**, B) experimental and simulated powder XRD profiles of **D2**. **D1** and **D2** were prepared by recrystallization from their solutions in DMF/H_2O = 9/1. C,D) are the simulated structures of **D1** and **D2**, respectively.

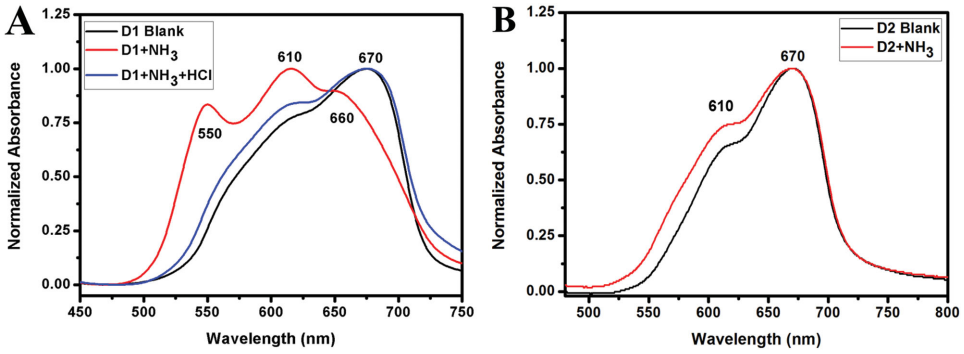

Figure 8. The UV–vis spectra of self-assembled A) **D1** and B) **D2** before and after treated with ammonia gas followed by the treatment with hydrochloric acid for 10 min and keep in vacuum for 30 min.

carboxylic acid and the carbonyl group of squaric acid and tends to aggregate into micro/nanoellipsoids. The XRD structural simulation, 2D NMR and FTIR analyses comfirm our hypothesis that the intermolecular hydrogen bonding and π–π stacking are the main driving forces for the aggregations of both **D1** and **D2**. Moreover, **D1** in the solid state showed selective reponse to ammonia gas due to its unique molecular aggregation and the size effect of ammonia molecule. The ammonia molecules can easily entered the **D1** aggregates due to their smaller size than the space of hydrogen-bonding network in **D1**, which breaks the hydrogen-bonding network and leads to the relative slide of **D1** molecules. The aggregated **D1** is then transferred from *J*-aggregation to *H*-aggreation. The hydrogen bonds and *J*-aggregation in **D1** can be easily recovered by the treatment with HCl gas. This unique property of **D1** makes it a promising candidate as reversible optical sensing material for ammonia gas.

4. Experimental Section

Materials and Methods: 4-Hydrazinobenzoic acid hydrochlorid (97%), 4-bromophenylhydrazine hydrochloride (97%), 3-methyl-2-butanone (98%), 4-bromomethylbenzoic acid (97%), and 3,4-dihydroxycyclobut-3-ene-1,2-dione (98%) were purchased from Alfa Aesar and used without further purifications. All solvents were dried prior to use with appropriate drying agents. Analytical thin layer chromatography was carried out on Yantai chemical industry silica gel plates and visualized by UV.

^{1}H, ^{13}C and 2D NMR spectra were recorded on a Bruker 400 (400 MHz ^{1}H; 100 MHz ^{13}C) or Bruker 600 (600 MHz ^{1}H; 150 MHz ^{13}C) spectrometer at room temperature. Mass spectra (MS) were measured with a XEVO-G2QTOF (ESI, Waters, USA). UV-visible spectra were obtained on a spectrometer (UV 2600, Shimadzu, Japan). Fluorescence spectroscopic studies were performed on a fluorescence spectrophotometer (Horiba Jobin Yvon FluoroMax-4 NIR, NJ, USA). Fourier transform infrared (FTIR) spectra were recorded with a Nicolet-50 DXC FTIR spectrophotometer and dry samples were

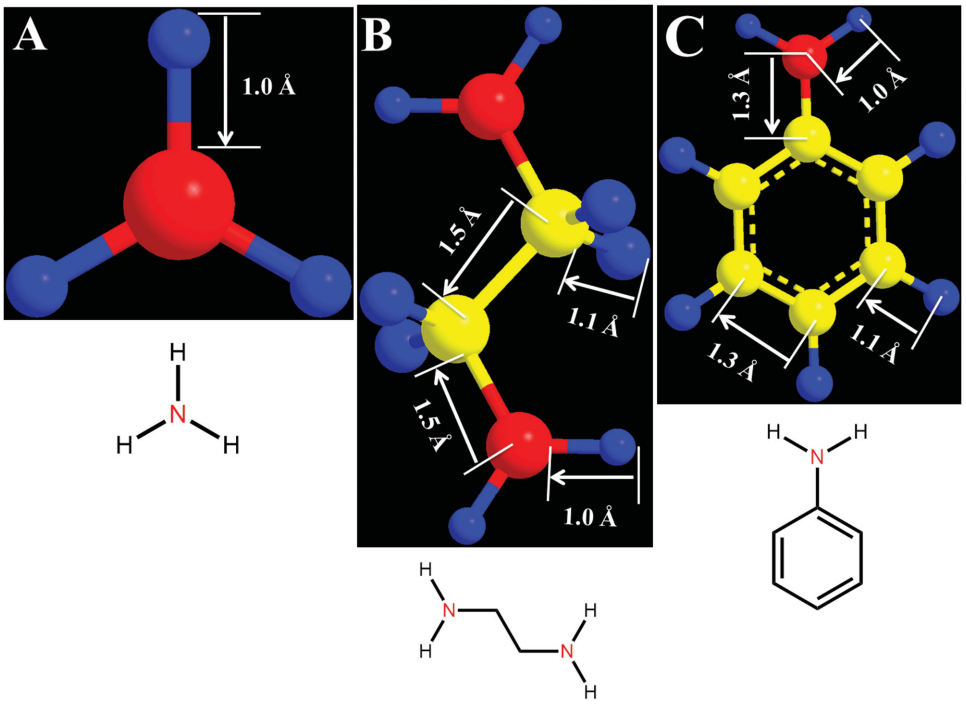

Figure 9. The structures of A) ammonia gas, B) ethanediamine gas, C) and aniline gas calculated using ChemDraw 3D in the lowest energy state. The blue, yellow, and red balls represent hydrogen atom, carbon atom, and nitrogen atom, respectively.

prepared as KBr pellets at room temperature. Powder XRD patterns were recorded on a D/max2500VB2+/Pc X-ray diffractometer (Rigaku) using Cu Kα radiation in the 2θ range 5°–20°. Morphologies of self-assembled **D1** and **D2** were observed with a Hitachi S-4700 scanning electron microscope (SEM), a JEOL JEM-3010 high resolution transmission electron microscope (HRTEM) and an Axioskop 40A Pol Optical Microscope (Carl Zeiss) POM.

*Preparing Self-Assembled **D1** and **D2***: The self-assembly of **D1** and **D2** was proceeded in DMF solution via a solvent evaporation method. The solid state UV–vis spectra were measured on a hydrophilic quartz matrix. The samples of **D1** and **D2** for morphologies were given as the same method on an appropriate matrix.

Computational Methods: The indexing of the peaks in the powder XRD pattern with a long-time scan was performed using the TREOR program[20] on the Reflex Powder Indexing module in Materials Studio software,[21] in which the crystal type and approximate lattice parameters can be determined from the peak positions by testing in six common space groups (cubic, hexagonal, tetragonal, orthorhombic, monoclinic, and triclinic). Then, the accurate lattice parameters of the sample were determined by Pawley fitting,[22] which can give the most likely triclinic space groups of the crystal system. The results show that **D1** and **D2** have a monoclinic lattice and the lattice parameters of a = 18.267 Å, b = 12.101 Å, c = 12.281 Å, α = 81.67°, β = 120.77°, γ = 110.4° for **D1** and a = 16.474 Å, b = 13.939 Å, c = 9.770 Å, α = 86.51°, β = 103.19°, γ = 115.83° for **D2**.

*Synthesis of **D1** and **D2***: **D1** and **D2** were obtained by three steps processes according to the previous literatures and the detailed reaction process was shown in Scheme S1 (Supporting Information).[23]

Supporting Information

Supporting Information is available from the Wiley Online Library or from the author.

Acknowledgements

This work was financially supported by the National Natural Science Foundation of China (21174012, 51221002, and 21574009), the Beijing Natural Science Foundation (2142026), and the Innovation and Promotion Project of Beijing University of Chemical Technology.

Received: September 9, 2015
Revised: October 12, 2015
Published online: November 24, 2015

[1] a) G. M. Whitesides, B. Grzybowski, *Science* **2002**, *295*, 2418; b) T. G. Barclay, K. Constantopoulos, J. Matisons, *Chem. Rev.* **2014**, *114*, 10217; c) M. Chen, M. Yin, *Prog. Polym. Sci.* **2014**, *39*, 365; d) K. Liu, Z. Xu, M. Yin*Prog. Polym. Sci.* **2015**, *46*, 25.

[2] a) H. Furukawa, J. Kim, N. W. Ockwig, M. O'Keeffe, O. M. Yaghi, *J. Am. Chem. Soc.* **2008**, *130*, 11650; b) J. M. Roberts, B. M. Fini, A. A. Sarjeant, O. K. Farha, J. T. Hupp, K. A. Scheidt, *J. Am. Chem. Soc.* **2012**, *134*, 3334.

[3] a) X. Chen, M. Addicoat, E. Jin, L. Zhai, H. Xu, N. Huang, Z. Guo, L. Liu, S. Irle, D. Jiang, *J. Am. Chem. Soc.* **2015**, *137*, 3241; b) D. Qu, Q. Wang, Q. Zhang, X. Ma, H. Tian, *Chem. Rev.* **2015**, *115*, 7543; c) P. Horcajada, R. Gref, T. Baati, P. K. Allan, G. Maurin, P. Couvreur, G. Ferey, R. E. Morris, C. Serre, *Chem. Rev.* **2012**, *112*, 1232; d) P. D. Frischmann, K. Mahata, F. Würthner, *Chem. Soc. Rev.* **2013**, *42*, 1847.

[4] a) J. Rabone, Y. F. Yue, S. Y. Chong, K. C. Stylianou, J. Bacsa, D. Bradshaw, G. R. Darling, N. G. Berry, Y. Z. Khimyak, A. Y. Ganin, P. Wiper, J. B. Claridge, M. J. Rosseinsky, *Science* **2010**, *329*, 1053; b) W. Li, L. Jin, N. Zhu, X. Hou, F. Deng, H. Sun, *J. Am. Chem. Soc.* **2003**, *125*, 12408.

[5] a) J. An, S. J. Geib, N. L. Rosi, *J. Am. Chem. Soc.* **2009**, *131*, 8376; b) M. Vallet-Regi, F. Balas, D. Arcos, *Angew. Chem. Int. Ed.* **2007**, *46*, 7548; c) P. Horcajada1, T. Chalati, C. Serre, B. Gillet, C. Sebrie, T. Baati, J. F. Eubank, D. Heurtaux, P. Clayette, C. Kreuz, J. Chang, Y. Hwang, V. Marsaud, P. Bories, L. Cynober, S. Gil, G. Férey, P. Couvreur, R. Gref, *Nat. Mater.* **2010**, *9*, 172.

[6] a) R. S. Stoll, N. Severin, J. P. Rabe, S. Hecht, *Adv. Mater.* **2006**, *18*, 1271; b) M. Matsui, M. Fukushima, Y. Kubota, K. Funabiki, M. Shiro, *Tetrahedron* **2012**, *68*, 1931.

[7] J. Yum, P. Walter, S. Huber, D. Rentsch, T. Geiger, F. Nüesch, F. D. Angelis, M. Grätzel, M. K. Nazeeruddin, *J. Am. Chem. Soc.* **2007**, *129*, 10320.

[8] a) G. Zhang, M. Liu, *J. Phys. Chem. B* **2008**, *112*, 7430; b) F. Fennel, S. Wolter, Z. Xie, P. Plötz, O. Kühn, F. Würthner, S. Lochbrunner, *J. Am. Chem. Soc.* **2013**, *135*, 18722.

[9] R. S. Grynyov, A. V. Sorokin, G. Y. Guralchuk, S. L. Yefimova, I. A. Borovoy, Y. V. Malyukin, *J. Phys. Chem. C* **2008**, *112*, 20458.

[10] a) S. R. Arepalli, C. P. Glaudemans, G. Daves, P. Kovac, A. Bax, *J. Magn. Reson. B* **1995**, *106*, 195; b) U. Mayerhöffer, F. Würthner, *Angew. Chem. Int. Ed.* **2012**, *51*, 5615.

[11] a) D. M. Eisele, C. W. Cone, E. A. Bloemsma, S. M. Vlaming, C. Kwaak, R. J. Silbey, M. G. Bawendi, J. Knoester, J. P. Rabe, D. A. V. Bout, *Nat. Chem.* **2012**, *4*, 655; b) J. M. Malicka, A. Sandeep, F. Monti, E. Bandini, M. Gazzano, C. Ranjith, V. K. Praveen, A. Ajayaghosh, N. Armaroli, *Chem. Eur. J.* **2013**, *19*, 12991.

[12] a) O. Gershevitz, C. N. Sukenik, *J. Am. Chem. Soc.* **2004**, *126*, 482; b) X. Cha, K. Ariga, T. Kunitake, *J. Am. Chem. Soc.* **1996**, *118*, 9545.

[13] a) K. Jeong, S. Jin, J. J. Ge, B. S. Knapp, M. J. Graham, J. Ruan, M. Guo, H. Xiong, F. W. Harris, S. Cheng, *Chem. Mater.* **2005**, *17*, 2852; b) J. Zhang, M. Zhou, S. Wang, J. Carr, W. Li, L. Wu, *Langmuir* **2011**, *27*, 4134.

[14] E. B. Adamska, Z. D. Szafran, A. Komasa, M. Szafran, *Chem. Phys.* **2014**, *444*, 7.

[15] a) D. Bučar, G. M. Day, I. Halasz, G. Z. Zhang, J. R. G. Sander, D. G. Reid, L. R. MacGillivray, M. J. Duer, W. Jones, *Chem. Sci.* **2013**, *4*, 4417; b) M. Frenette, G. Cosa, T. Friščić, *CrystEngComm* **2013**, *15*, 5100.

[16] A. Kaushik, R. Kumar, S. K. Arya, M. Nair, B. D. Malhotra, S. Bhansali, *Chem. Rev.* **2015**, *115*, 4571.

[17] a) D. Britt, D. Tranchemontagne, O. M. Yaghi, *Proc. Natl. Acad. Sci. USA* **2008**, *105*, 11623; b) N. B. Shustova, A. F. Cozzolino, S. Reineke, M. Baldo, M. Dinca , *J. Am. Chem. Soc.* **2013**, *135*, 13326.

[18] Z. Yan, H. Xu, S. Guang, X. Zhao, W. Fan, X. Liu, *Adv. Funct. Mater.* **2012**, *22*, 345.

[19] a) J. Li, R. J. Kuppler, H. Zhou, *Chem. Soc. Rev.* **2009**, *38*, 1477; b) J. L. C. Rowsell, E. C. Spencer, J. Eckert, J. A. K. Howard, O. M. Yaghi, *Science* **2005**, *309*, 1350.

[20] P. E. Werner, L. Eriksson, M. Westdahl, *J. Appl. Crystallogr.* **1985**, *18*, 367.

[21] Reflex Module, MS Modeling, Version 2.2, Accelrys Inc. San Diego, CA 2003.

[22] A. J. Markvardsen, W. I. F. David, J. C. Johnson, K. Shankland, *Acta Cryst.* **2001**, *57*, 47.

[23] a) J. Li, K. Guo, J. Shen, W. Yang, M. Yin, *Small* **2014**, *10*, 1351; b) J. Li, C. Ji, W. Yang, M. Yin, *Analyst* **2013**, *138*, 7289; c) C. Ji, Y. Zheng, J. Li, J. Shen, W. Yang, M. Yin, *J. Mater. Chem. B* **2015**, *3*, 7494.